ISSN: 0067-3064

Physical properties of the perovskite MoMnO3 by DFT method

S. El Kamli[1], Y. Selmani[1], A. Jabar[2,3], S. Benyoussef [1], L. Bahmad [1,*] and A. Kassou-Ou-Ali[1]

[1] Laboratory of Condensed Matter and Interdisciplinary Sciences (LaMCScI), Faculty of Sciences, Mohammed V University, Av. Ibn Batouta, B. P. 1014 Rabat, Morocco

[2] LPHE-MS, Science Faculty, Mohammed V University in Rabat, Morocco

[3] LPMAT, Faculty of Sciences Aïn Chock, Hassan II University of Casablanca, B.P. 5366 Casablanca, Morocco

*Corresponding author: l.bahmad@um5r.ac.ma (L.B.)

Abstract

The present work uses first-principles methods to investigate the structural, electronic, optical, and thermoelectric properties of the perovskite $MoMnO_3$. This research utilizes density functional theory (DFT) within the Wien2k code. The structure of $MoMnO_3$ has a trigonal symmetry, with typical lattice parameters of $a_0 = b_0 = 5.456$ Å and $c_0 = 14.867$ Å. The electronic results show that $MoMnO_3$ is a semiconductor with a majority spin energy gap of approximately 0.333 eV and a minority spin energy gap of around 1.987 eV, allowing good light absorption. While, the valence band is mainly composed of the 3d manganese orbitals, while the 4d molybdenum orbitals dominate the conduction band. The analysis of the high absorption coefficient shows that this optical absorption is important in the visible and near-infrared range. $MoMnO_3$ has a non-negligible power factor at room temperature. These results clearly show that this perovskite has specific and interesting physical properties that offer numerous advantages for applications in fields such as electronics, energetics, optoelectronics and spintronics.

Keywords: DFT calculations; physical properties; perovskite; oxide $MoMnO_3$; electronic properties; optical properties.

1. Introduction

Recently, a new class of materials called perovskites has emerged due to their multiple applications. These materials exhibit interesting magnetic, optical, electronic and catalytic properties [1-7], attracting the attention of many applications. Moreover, perovskite oxides have an ABO_3-type chemical formula, where the A site contains alkaline earth metals (e.g. Ca, Sr, etc.) or rare earth elements (e.g. Y, La, Er, Sm, Dy, etc.), while the B sites in the structure host transition metal elements like Ti, Cr, Mn, Co, and Fe, making them effective choices for applications in magnetic refrigeration, Spintronic and fuel cells, etc., due to their considerable activity [8-14].

Lanthanide-based perovskite $LaMO_3$ (where M= Fe, Co, Mn, etc.) with orthorhombic structure have been studied enormously and have emerged as promising candidates for a vast array of applications, spanning catalysis [15, 16], Spintronic [17], optoelectronics [18], sensors [19] and oxide fuel cells [20]. In addition, $REMnO_3$ rare-earth-based multi-ferroic manganites are of great scientific interest due to their interesting electronic, optical and magnetic, magnetocaloric properties [21-24]. Certain studies have demonstrated that REMnO3 materials are among the most promising magnetocaloric materials for applications [25-29]. However, other studies show an interesting coupling between magnetic and electrical properties, which is of interest for several applications such as Spintronic [30-34].

Multiferroic manganite $HoMnO_3$ was instigated using non-collinear spin density functional theory to explore their potential for use in photovoltaic applications [35]. On the other hand, it should be noted from a previous study that the antiferromagnetic transition temperature (T_N) of the hexagonal $HoMnO_3$ crystal is 72 K, while its ferroelectric transition temperature (T_C) is 875 K [36, 37]. B. Bouadjem *et al.* [38] have investigated the electronic, magnetic and optical properties of the orthorhombic perovskite oxide $NdMnO_3$. The results obtained in this study make orthorhombic $NdMnO_3$ a promising candidate for applications in Spintronic and optoelectronics. $RMnO_3$ manganite perovskites (where R = Gd and Tb) have been extensively studied in terms of their ferroelectric and magneto-electric physical properties [39, 40]. Theoretical studies of $PrMnO_3$'s structural, electronic and magnetic properties reveal its semi-metallic nature in the orthorhombic crystal [41, 42].

$MoMnO_3$ is a ternary oxidized compound composed of molybdenum (Mo), manganese (Mn) and oxygen (O). Its crystal structure belongs to the perovskite family, known for its diverse properties. This compound exhibits interesting physical phenomena, such as multi-

ferroicity and magnetism, making it a fascinating material for both fundamental research and technological applications. In addition, DFT calculations can shed light on the coupling between magnetic and ferroelectric properties in multi-ferroic $MoMnO_3$.

This study aims to explore the physical properties of $MoMnO_3$, including the structural, electronic, magnetic and optical properties of $MoMnO_3$ perovskites. These calculations were carried out using DFT theory as implemented in the computer simulation code. As a result, this investigation will aid in improving comprehension of the fundamental characteristics of the novel $MoMnO_3$ manganite perovskites. This knowledge paves the way for new applications and the exploitation of $MoMnO_3$'s unique properties in advanced technological fields.

2. Computational methods

As part of this investigation, particular attention will be paid to the structural, electronic, optical and thermoelectric properties of the $MoMnO_3$ material. These properties were computed through the full-potential linearized augmented plane wave technique FP-LAPW [43, 44] based on DFT theory as employed in the Wien2K simulation code. The exchange and correlation potential were calculated using the generalized gradient approximation (GGA) according to the parameterization of Perdew, Burke and Ernzerhof (PBE) [45]. To study the effect of spin-orbit coupling (SOC) as well as Hubbard potential (U) on the electronic and magnetic properties of $MoMnO_3$, U_{eff} = U-J = 3.9 eV for Mn and 4.38 eV for Mo were performed. The Hubbard correction has been used to account for Coulomb interactions between electrons in Mo and Mn atoms [46]. To ensure the separation of the core and valence states, the cut-off energy was set at -6.0 Ry. To control the size of plane-wave basis sets, the kinetic energy cutoff was set to $R_{MT} \times K_{MAX}$ = 9.0. For all of our computations, we have also selected a 10 × 10 × 10 k-points mesh for the Brillouin zone integration. Furthermore, the thermoelectric characteristics of the considered material were investigated by combining electronic band structure results and Boltzmann transport theory as implemented in the BoltzTraP simulation program [47].

3. Results and discussion

3.1. Crystal structure and structural properties

Using the DFT theory with GGA+SOC+U approaches, the structural, electronic, optical and thermoelectric properties of $MoMnO_3$ material have been investigated. The $MoMnO_3$ perovskite has a trigonal crystal structure with the space group R-3 (N° = 148). The structure of this system, illustrated in Figure 1, consists of Mo, Mn and O with the electronic configuration [Kr] $4d^5 5s^1$, [Ar] $3d^5 4s^2$ and [He] $2s^2 2p^4$, respectively. The atomic positions of each element making up the $MoMnO_3$ material are shown in Table 1.

The structural properties are studied in depth to optimize key parameters such as the lattice constants, the modulus of elasticity, and the pressure-induced phase transitions for both the ferromagnetic (FM) and the antiferromagnetic (AFM) orders of the material under investigation. These parameters are optimized using the empirical Birch-Murnaghan equation of state [48]. The obtained results are summarized in Table 2. This table clearly shows that $E_{AFM} < E_{FM}$. The result suggests that the AFM phase is more energetically interesting than the FM phase, making it the configuration of the stable ground state for the candidate compound. In addition, the equilibrium lattice parameters for the hexagonal perovskite $MoMnO_3$ in the FM and AFM states are as follows: $a_0 = b_0 = 5.456$ Å and $c_0 = 14.867$ Å.

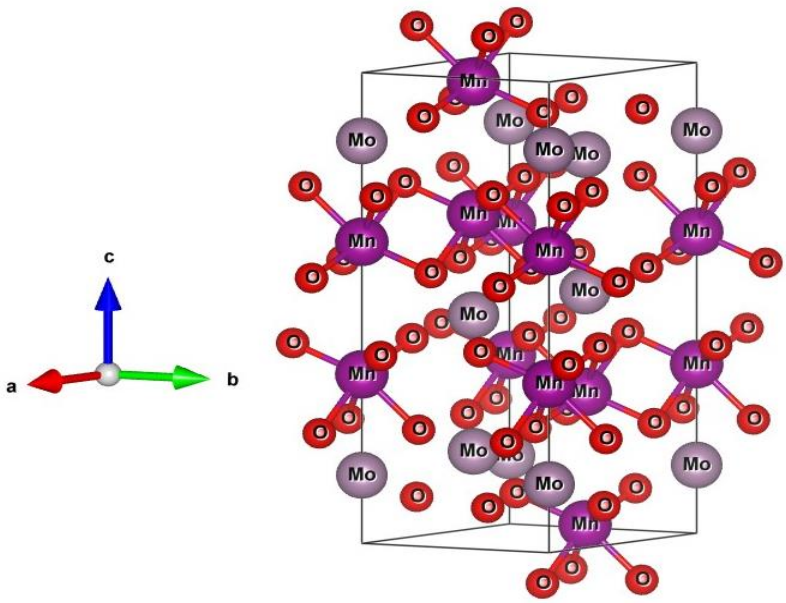

Fig. 1*: The crystal structure of $MoMnO_3$, obtained using Vesta software [49].*

Table 1. *The atomic positions of the perovskite $MoMnO_3$.*

Atoms	x	y	z
Mo	0.66667	0.33333	0.47824
Mn	0.00000	0.00000	0.64080
O	0.34761	0.37457	0.41995

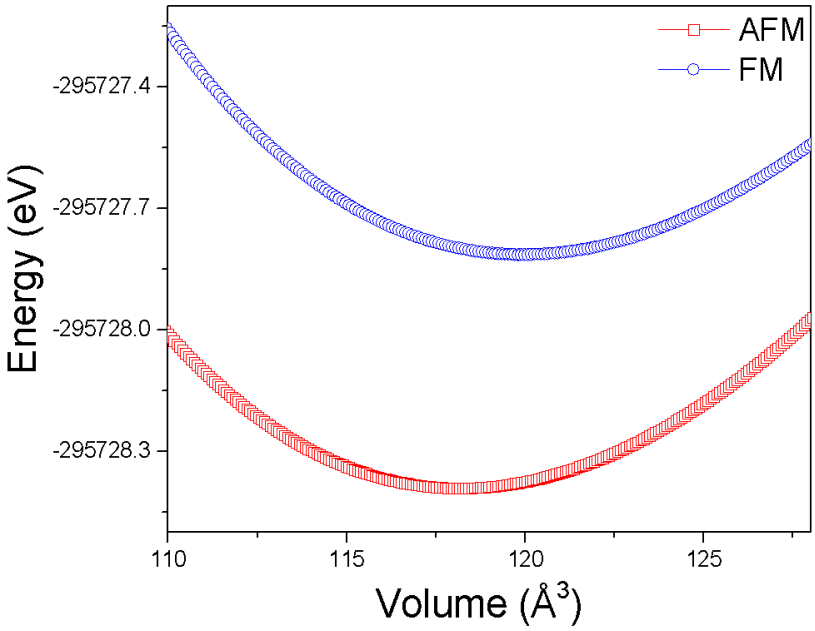

Fig. 2*: The energy vs. the volume of the $MoMnO_3$ compound.*

Table 2: *Calculated equilibrium lattice parameters, such as: volume V_0 (in Å^3), bulk modulus B_0 (in GPa), its first pressure derivative B' and the minimum total energy E_0 (in eV) for the trigonal $MoMnO_3$ compound by employing the GGA+SOC+U approximation.*

State	V_0(Å^3)	B_0(GPa)	B'	E_0(eV)
FM	119.949	182.682	4.649	- 295728.391
AFM	118.209	186.842	4.406	- 295727.815

3.2 Electronic properties

To explore the electronic characteristics of the trigonal system $MoMnO_3$, we employed the optimized lattice parameters $a_0 = b_0 = 5.456$ Å and $c_0 = 14.867$ Å, which were derived from the assessment of the structural properties. The GGA+SOC+U approximation was employed to compute the total and partial densities of states for $MoMnO_3$ in an antiferromagnetic configuration between the Mo and Mn ions. These results are presented in Figure 3. The figure demonstrates the semiconducting properties of the studied material, featuring a majority spin energy gap of approximately 0.333 eV and a minority spin energy gap of around 1.987 eV.

We also note that $MoMnO_3$ material are magnetic, due to the asymmetry between major and minor spin states. This is also confirmed by the partial moments shown in Table 3, which are calculated in this work. Furthermore, at majority spins, the maximum value point of the valence band (MVB) and the minimum value of the conduction band (MCB) are dominated by Mo-d with O-p states. In the case of minority spins, the MVB band is mainly formed by Mn-p and Mo-d orbitals, while Mo-d hybridizes with O-p states to form the MCB band.

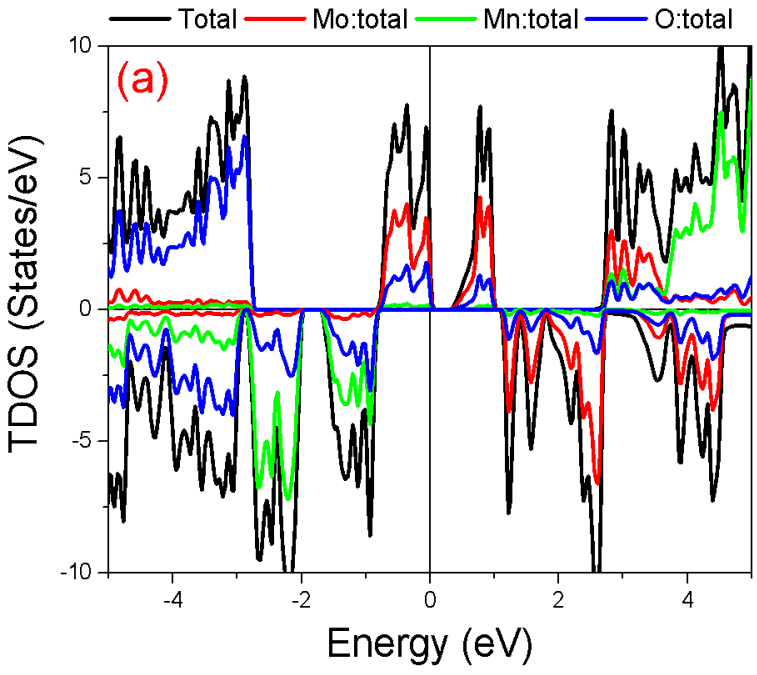

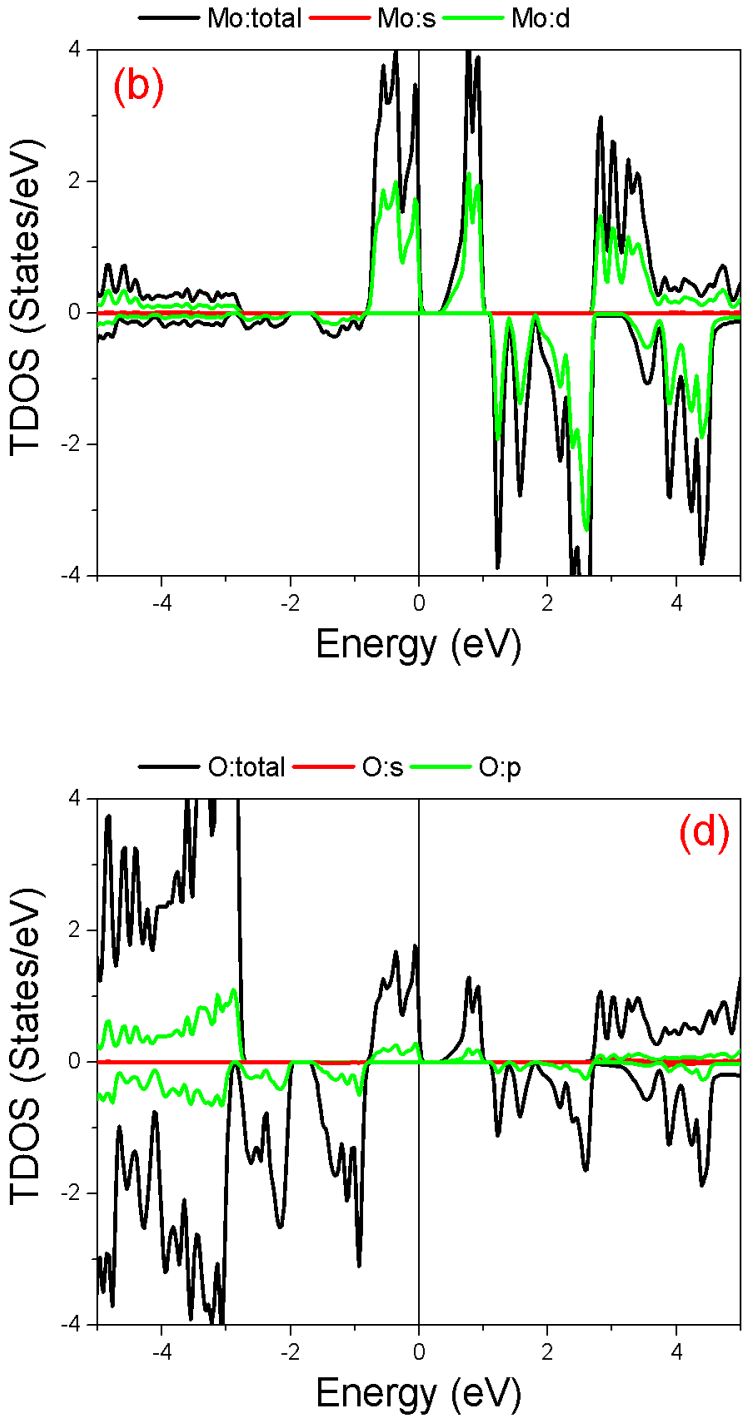

Fig.3: *The computed densities of states: (a) total density of state (TDOS) and (b, c and d) the partial density of state (PDOS) of $MoMnO_3$ using GGA+SOC+U approach.*

Table 3: *The calculated partial magnetic moments (in μ_B) and band gap (eV) of the $MoMnO_3$ compound by using GGA+SOC+U approximation.*

$M_{Mo}(\mu_B)$	$M_{Mn}(\mu_B)$	$M_O(\mu_B)$	E_g(eV)-Up	E_g(eV)-Down
1.21694	-4.40208	0.01324	0.333	1.987

3.3 Optical properties

For investigating the optical behavior of $MoMnO_3$ material, the dielectric function includes optical parameters such as real part $\varepsilon_1(\omega)$ and the imaginary part $\varepsilon_2(\omega)$ and the refractive index $n(\omega)$, optical absorption $\alpha(\omega)$, reflectivity $R(\omega)$, energy loss function $L(\omega)$, real $\sigma_1(\omega)$ and imaginary $\sigma_2(\omega)$ parts of optical conductivity, were examined against photon energy.

Initially, the real and imaginary parts of the dielectric function were calculated using the GGA+SOC+U approximation within the Kramers-Kronig expressions [50]:

Imaginary part of dielectric constant $\varepsilon_2(\omega)$:

$$\varepsilon_2(\omega) = \frac{4\pi^2 e^2}{m^2\omega^2}\sum_{i,j}\int_{Bz} < i|M|j >^2 \times f(i)(1-f(i))\delta(E_{j,k} - E_{i,k} - \omega)d^3k \qquad \textbf{(1)}$$

Where ***M*** represents the dipole matrix, ***i*** and ***j*** are initial and final states, respectively. The ***m, e,*** **ω** and **k** parameters stand for the mass, the charge of the electron, frequency and the crystal wave vector, respectively. While $f(i)$ is the Fermi distribution function, $\boldsymbol{E_{x,y}}$ denote the free electron energy.

Real part of dielectric constant $\varepsilon_1(\omega)$:

$$\varepsilon_1(\omega) = 1 + \frac{2}{\pi}P\int_0^\infty \omega'\,\varepsilon_2(\omega').\frac{d\omega'}{\omega'^2-\omega^2} \qquad \textbf{(2)}$$

Where P stands for the principal value of the integral.

On the other hand, the optical coefficients including $\alpha(\omega)$, $L(\omega)$, $\sigma_1(\omega)$, $\sigma_2(\omega)$, $n(\omega)$ and $k(\omega)$ are needed to study the optical behavior of the studied materials for various applications in optoelectronics and other related devices. These parameters are obtained from $\varepsilon_1(\omega)$ and $\varepsilon_2(\omega)$ using the following mathematical formulas [51, 52]:

$$\alpha(\omega) = \frac{\sqrt{2}\omega}{C}\left([\varepsilon_1^2(\omega) + \varepsilon_2^2(\omega)]^{\frac{1}{2}} - \varepsilon_1(\omega)\right)^{\frac{1}{2}} \qquad \textbf{(3)}$$

$$L(\omega) = \frac{\varepsilon_2(\omega)}{\varepsilon_2^2(\omega) + \varepsilon_1^2(\omega)} \qquad \textbf{(4)}$$

$$\sigma_1(\omega) = \frac{\omega\varepsilon_2}{4\pi} \qquad \textbf{(5)}$$

$$\sigma_2(\omega) = -\frac{\omega\varepsilon_1}{4\pi} \quad \textbf{(6)}$$

$$n(\omega) = \frac{1}{\sqrt{2}}\left([\varepsilon_1^2(\omega) + \varepsilon_2^2(\omega)]^{\frac{1}{2}} + \varepsilon_1(\omega)\right)^{\frac{1}{2}} \quad \textbf{(7)}$$

$$k(\omega) = \frac{1}{\sqrt{2}}\left([\varepsilon_1^2(\omega) + \varepsilon_2^2(\omega)]^{\frac{1}{2}} - \varepsilon_1(\omega)\right)^{\frac{1}{2}} \quad \textbf{(8)}$$

Figs. 4(a) and 4(b) represent the evolution of the real $\varepsilon_1(\omega)$ and the imaginary $\varepsilon_2(\omega)$ parts of the dielectric function in an energy range [0-13.5 eV] for the $MoMnO_3$ compound. It is well known that the real part $\varepsilon_1(\omega)$ of the dielectric function describes the polarization of the crystal, and it determines the propagation speed of electromagnetic waves in the material. Fig. 4(a) clearly shows that the initial sharp peaks of the real dielectric constant for the $MoMnO_3$ compound are observed in the visible range. At zero frequency, we notice that the static dielectric constant value is 10.48, 10.48 and 6.31 along the xx, yy and zz directions, respectively. In Fig. 4(a), we notice that the intensity is initially maximum at the energy point of 0.5 eV, and then it decreases. The spectrum of $\varepsilon_1(\omega)$ also cancels out at a point corresponding to an energy value of 7.5 eV. Then it decreases and takes negative values up to an energy point of 9 eV, and it presents major peaks in the UV and visible domains.

The computed imaginary part of the dielectric function versus energy is depicted in Fig. 4(b). We observe that the spectrum of the dielectric function at 0.5 eV is maximal, and it also presents major peaks. At photon energy of 7.5 eV, the $\varepsilon_1(\omega)$ cancels out and the $\varepsilon_2(\omega)$ reaches a maximum value at the initial peak. Beyond this value, the real part of the dielectric function decreases and becomes negative and the imaginary part of this function decreases rapidly and becomes weak.

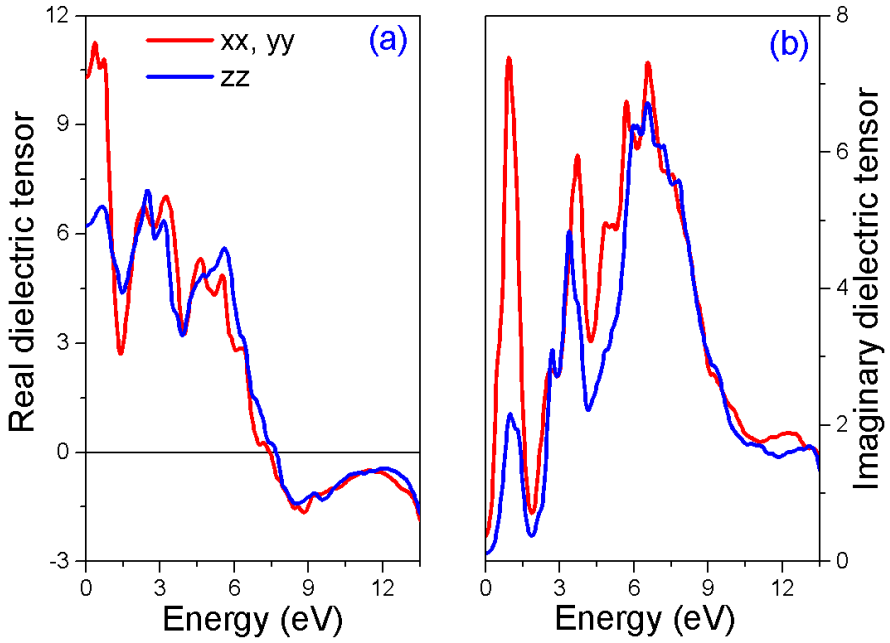

Fig.4: *(a) The real and (b) imaginary parts of the dielectric function for $MoMnO_3$.*

The absorption coefficient of a material is a measure of its ability to absorb electromagnetic waves such as light. In the visible range at low photon energies (<4.5ev) the compound shows weak peaks, so it has minimal absorption of the violet and blue colors of visible light and after (>4.5ev) shows higher absorption values for other colors green, yellow, orange, red. Both the photon-electron interactions within the atoms and the structural characteristics of $MoMnO_3$ can cause the absorption peak to shift from lower to higher energy levels.

The absorption spectra are shown in Fig. 5(a). The absorption threshold begins at E=0.5eV. In the range (0.5-2eV) a peak is observed, then the absorption coefficient increases regularly with the energy of the incident photons. A major peak is observed in the range (3.5-4.5eV), and the highest absorption peak occurs at 8.5eV in the UV region. More precisely, the perovskite $MoMnO_3$ shows dominance in the transition between the UV and visible spectra.

Fig.5 (b): The evolution of the energy loss function of the $MoMnO_3$ material is represented in Fig.5 (b). This pattern shows 2 major peaks and reaches a maximum value near the energy point 10.5 eV, then it decreases. This energy loss strongly depends on the absorption coefficient of the material.

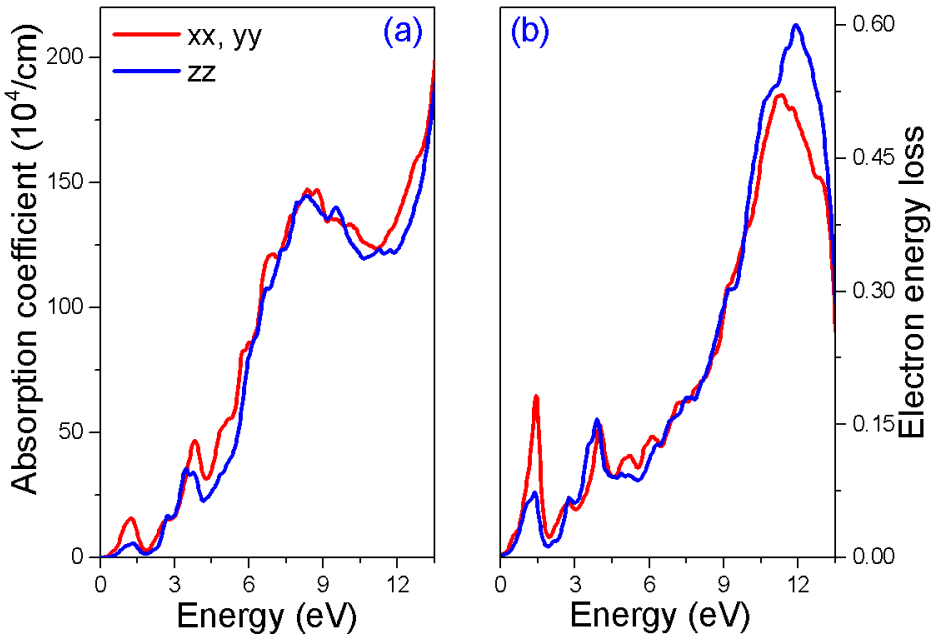

***Fig.5**: The absorption coefficient (a), the electron energy loss (b) for $MoMnO_3$.*

The optical conductivity is a complex quantity, and the patterns of the real and imaginary components of the optical conductivity are represented in Fig.6 (a) and (b). The calculations are done using the equation Eqs. (5 and 6) in the energy range [0, 13.5 eV]. The real optical conductivity shows significant and maximum peaks at the energy point of 7.5 eV. At this point, the $MoMnO_3$ material conducts electric current. It is observed that the real part of the optical path reaching its maximum corresponds to the imaginary part being at its minimum, and vice versa, with the imaginary part also becoming negative. The imaginary optical conductivity presents a minimum, which means that the energy storage in $MoMnO_3$ is low, so it disperses light. The optical conductivity of the $MoMnO_3$ perovskite is primarily determined by the inter-band transitions involving the valence and conduction electrons.

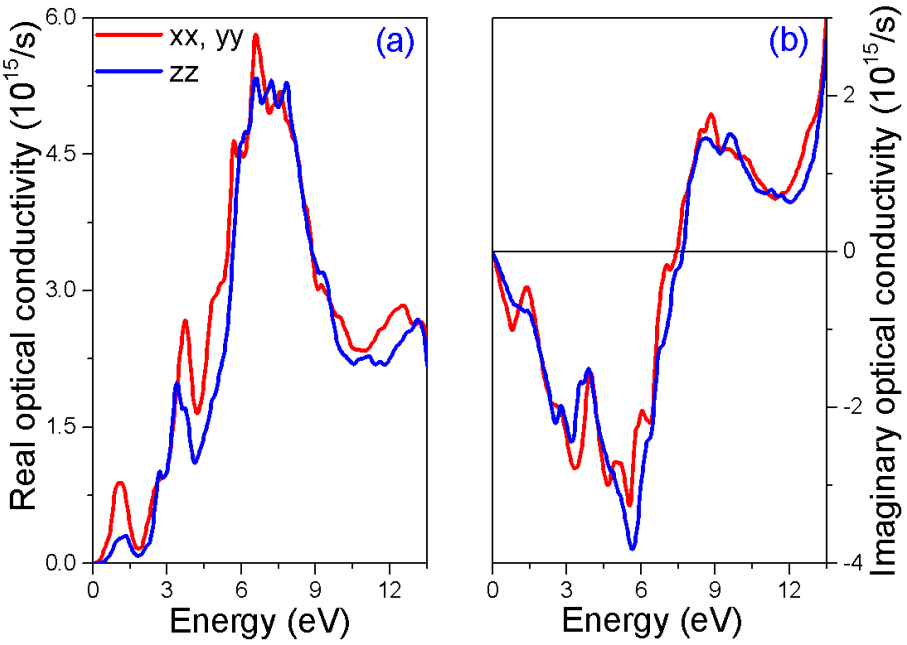

Fig. 6: *(a) the real and (b) imaginary parts of optical conductivity for* $MoMnO_3$.

The refractive index characterizes the propagation speed of a light radiation in the material and is directly related to the dielectric value of the material. Initially, the $MoMnO_3$ compound has a higher refractive index due to its narrow band gap and high electron density. This results in a strong interaction between light and the material. The refractive index depends on the polarization of the magnetic field of an electromagnetic wave at the surface of the material. The absorption coefficient is inversely related to the refraction coefficient, the lower the refraction index, the lighter the material absorbs. The extinction coefficient of a material is a measure that characterizes the material's ability to absorb an electromagnetic wave at a particular wavelength.

The structure of the material causes photons to be scattered in different directions, and this scattering is more likely to occur at shorter wavelengths (higher photon energies) because the scattering centers are smaller compared to the light's wavelength. As photon energy increases, both scattering and absorption tend to increase, leading to an overall rise in the material's extinction coefficient.

.

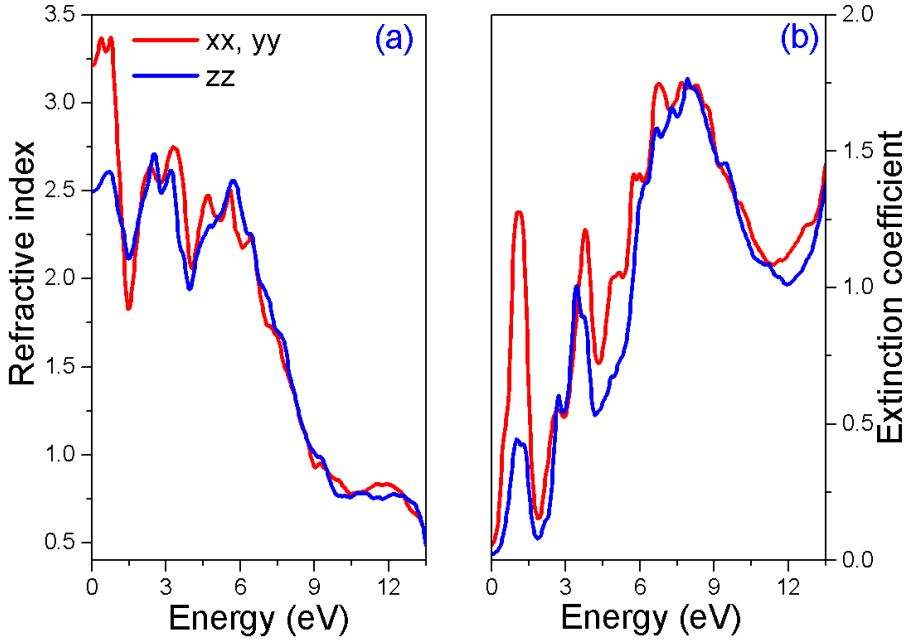

Fig. 7: *The refractive index (a) and the extinction coefficient (b) for* $MoMnO_3$.

3.4 Thermoelectric properties

The thermoelectric properties of the compounds are examined for potential applications in energy conversion, thermoelectric refrigeration, computer cooling, and miniature detector components. The thermoelectric effect is driven by the generation of a potential difference, which subsequently creates a heat gradient. To calculate the necessary transport quantities, such as electrical conductivity (σ/τ), Seebeck coefficient (S), electronic thermal conductivity (κ_e/τ), and the power factor (PF) as a function of temperature, we employed the BoltzTraP code interfaced with WIEN2k. The relaxation time τ depends, in principle, on both the wave vector and frequency. However, BoltzTraP treats the relaxation time to be a constant, which is a reasonable assumption. Our calculations for all TE properties were performed with a constant relaxation time approximation $\tau = 10^{-14}s$, which is the value often chosen in similar calculations [53-54].

The Seebeck coefficient is a measure of the intrinsic capacity of a material to generate an electrical voltage under the effect of a thermal gradient. The Seebeck coefficient (S) of $MoMnO_3$ within the temperature range from 10 to 800 K is shown in Fig. 8(a). The curve of S starts to increase with the increase in temperature to reach the maximum value is 230 $\mu V/K$

obtained at 100 K then it decreases. The increase in S is attributed to a perfect concentration of the holes where the Seebeck coefficient begins to increase as the temperature increases. The positive Seebeck coefficient indicates that $MoMnO_3$ is a p-type material. This high value indicates that $MoMnO_3$ has a high thermoelectric power, making it an interesting material for thermoelectric applications. The variation of electrical conductivity with temperature is shown in the Fig. 8(b). The electrical conductivity (σ/τ) increases sharply with increasing temperature to reach the maximum value is $0.165 \times 1020\, \Omega^{-1}.m^{-1}.s^{-1}$ obtained at 800 K. This behavior indicates the semiconducting nature of $MoMnO_3$.Similar results were found previously [54]. The electronic part of thermal conductivity (κ_e/τ) within the temperature range from 10 to 800 K is illustrated in Fig. 8(c). The curve increases very fast with the temperature. The electronic part of the thermal conductivity is therefore fairly low, which is favorable for thermoelectric performance. The power factor $(s^2\sigma/\tau)$ is an interesting parameter for assessing the thermoelectric performance of a material and is illustrated in Fig. 8(d) for $MoMnO_3$. The power factor rises rapidly with increasing temperature, reaching a maximum value of 3.2×10^{14} at 800 K. These results show the thermoelectric performance of the $MoMnO_3$ compound at high temperatures.

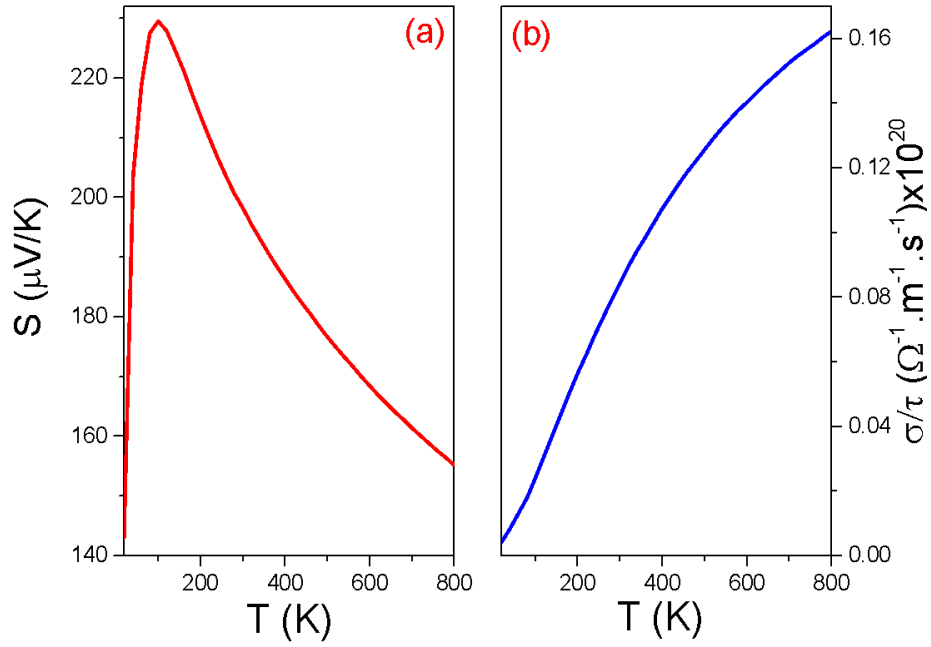

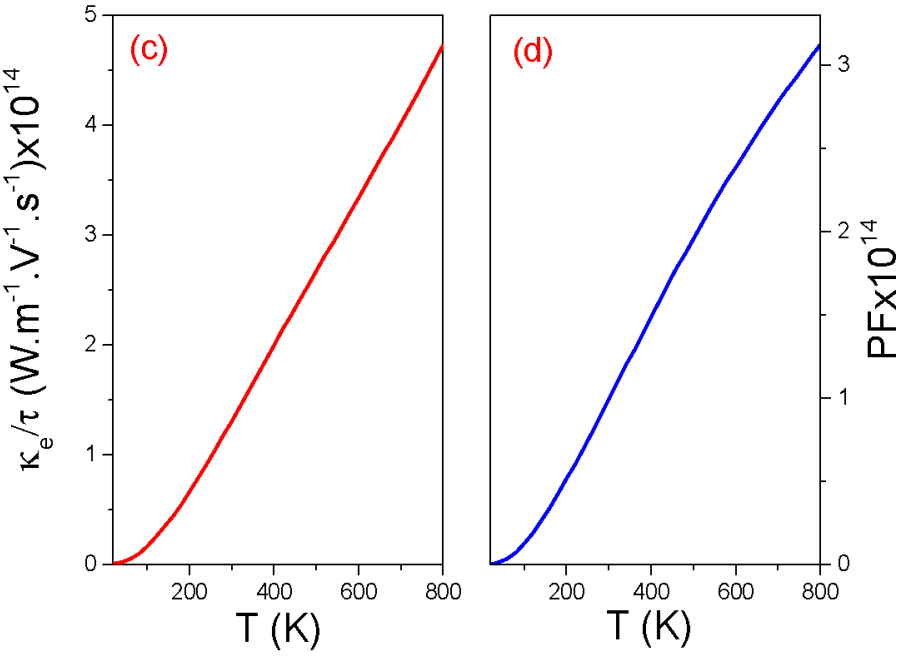

Fig. 8: *Seebeck thermoelectric coefficient (a), electrical conductivity (b), electronic component of thermal conductivity (c) power factor (d) of $MoMnO_3$ by using GGA+SOC+U approach.*

4. Conclusion

The present theoretical work involves the study of the physical properties of a typical material, $MoMnO_3$, in the framework of DFT theory employing the GGA+SOC+U approximation. Structural optimization has confirmed that the compound studied belongs trigonal structure with lattice constant values of $a_0 = b_0 = 5.456$ Å and $c_0 = 14.867$ Å. In addition, the semiconducting character with a non-zero band gap of the compound under study is justified by the densities of electronic states. Moreover, the non-symmetric nature between minority and majority spins describes the magnetic characteristic of the material. Concerning the optical properties, evaluating the complex dielectric constant helped us to identify other fundamental optical characteristics, namely the refractive index, reflectivity and extinction coefficient. We found that these materials have a high absorption in the energy range of 6.0-12 eV. In addition, the calculations established the zero-frequency value of the dielectric constant $\varepsilon_1(0)$, the refractive index $n(0)$ and the reflectivity $R(0)$. These materials appear to have promising

potential for applications in systems operating in the visible-ultraviolet parts of the electromagnetic spectra. A crucial aspect of our current research concerns the thermoelectric response of these compounds. Our results indicate that $MoMnO_3$ has good thermal and electrical conductivity and a higher power factor. Our study concludes that the perovskite oxide $MoMnO_3$ could be a potential candidate for use in Spintronic, thermoelectric and optoelectronic applications.

Declarations:

Funding:

The authors have received no funding to accomplish this work.

Conflicts of interest:

The authors declare no conflict of interest.

Data availability statement:

No data are associated with this article.

Author contribution statement:

Conceptualization, S. E. K.; Software, A. J.; Validation, L. B. and A. K.-O.-A.; Formal Analysis, S. B. and L. B.; Investigation, A. J.; Resources, L. B.; Data Curation, S. B.; Writing − Original Draft Preparation, S. E. K.; Writing − Review and Editing, L. B., S. B. and A. J.; Visualization, S. B.; Supervision, L. B.; Project Administration, A. K.-O.-A.

References

[1] K.-I. Kobayashi, T. Kimura, H. Sawada, K. Terakura and Y. Tokura, Room-temperature magnetoresistance in an oxide material with an ordered double-perovskite structure, Nature, 395 (1998) 677-680.

[2] M. Rashid, Z. Abbas, and M. Yaseen, Theoretical investigation of cubic $BaVO_3$ and $LaVO_3$ Perovskites via Tran–Blaha-modified Becke–Johnson exchanges potential approach, J Supercond Nov Magn, 30 (2017) 3129-3136.

[3] Y. Selmani, H. Labrim, M. Mouatassime, and L. Bahmad, Structural, optoelectronic and thermoelectric properties of Cs-based fluoro-perovskites $CsMF_3$ (M= Ge, Sn or Pb), Materials Science in Semiconductor Processing 152 (2022) 107053.

[4] Chuanhui Zhang, Haijie Cao, Chao Wang, Maoxia He, Wangcheng Zhan, and Yanglong Guo, Catalytic mechanism and pathways of 1, 2-dichloropropane oxidation over $LaMnO_3$ perovskite: An experimental and DFT study. Journal of Hazardous Materials, 402 (2021) 123473.

[5] Jonathan Hwang, Reshma R. Rao, Livia Giordano, Yu Katayama, Yang Yu, and Yang Shao-Horn, Perovskites in catalysis and electrocatalysis, Science, 358.6364 (2017) 751-756.

[6] R. Terki, H. Feraoun, G. Bertrand, and H. Aourag, Full potential calculation of structural, elastic and electronic properties of $BaZrO_3$ and $SrZrO_3$, Phys Status Solidi B, 242 (2005) 1054-1062.

[7] C. E. Runge, A. Kubo, B. Kiefer, Y. Meng, V. B. Prakapenka, G. Shen, R. J. Cava and T. S. Duffy, Equation of state of $MgGeO_3$ perovskite to 65 GPa: comparison with the post-perovskite phase, Phys Chem Minerals, 33 (2006) 699-709.

[8] Zahid Ali, Imad Khan, Iftikhar Ahmad, M. Salman Khan, and S. Jalali Asadabadi, Theoretical studies of the paramagnetic perovskites $MTaO_3$ (M=Ca, Sr and Ba), Mater. Chem. Phys., 162 (2015) 308-315.

[9] Y. Selmani, M. Mouatassime, F. Goumrhar, H. Labrim, L. Bahmad, and A. Benyoussef, Structural, electronic and magnetic properties of the perovskite $YMnO_3$, Solid State Communications, 328 (2021)114254.

[10] Shahid Mehmood, Zahid Ali, Imad Khan and Iftikhar Ahmad, Effects of Ni substitution on the electronic structure and magnetic properties of perovskite $SrFeO_3$, Journal of Electronic Materials, 49 (2020) 3780-3790.

[11] Z. Ali, and A. Iftikhar, Band profile comparison of the cubic perovskites $CaCoO_3$ and $SrCoO_3$, Journal of electronic materials, 42 (2013) 438-444.

[12] S. Belhamra, R. Masrour, A. Jabar, and E. K. Hlil, A comparative study of the structural, electronic, magnetic properties and magnetocaloric effect of perovskite $LaRO_3$ (R= Mn, Cr and Fe). Polyhedron, 193 (2021) 114891.

[13] Jaka Sunarso, Angel A. J. Torriero, Wei Zhou. Patrick C. Howlett and M Forsyth, Oxygen reduction reaction activity of La-based perovskite oxides in alkaline medium: a thin-film rotating ring-disk electrode study, The Journal of Physical Chemistry C, 116 (2012) 5827-5834.

[14] J. Zamora, T. Bautista, N. S. Portillo-Vélez, A. Reyes-Montero, H. Pfeiffer, F. Sánchez-Ochoa, and H. A. Lara-García., Magnetic/optical assessments of $RFeO_3$ (R=La, Pr, Nd, and Sm) ceramics: An experimental and theoretical discernment, 971 (2024) 172646.

[15] Xuchen Yan, Jing Liu, Yingju Yang, Zhen Wang, and Ying Zheng, A catalytic reaction scheme for NO reduction by CO over Mn-terminated $LaMnO_3$ perovskite: A DFT study. Fuel Processing Technology, 216 (2021) 106798.

[16] C. Zhang, H. Cao, C Wang, M He, W Zhan, and Y Guo, Catalytic mechanism and pathways of 1, 2-dichloropropane oxidation over $LaMnO_3$ perovskite: An experimental and DFT study. Journal of Hazardous Materials, 402 (2021) 123473.

[17] S. Tariq, A. A. Mubarak, F. Hamioud, S Zahra, B Kanwal, and Q Afzal, Repercussion of pressure on thermodynamic, optoelectronic, thermoelectric and magneto-elastic rectitude of cubic $LaFeO_3$: quantum DFT perspective. Journal of Alloys and Compounds, 831 (2020) 154600.

[18] B. Sabir, G. Murtaza, and RMA Khalil, Ab-initio prediction of structure stability, electromagnetic, optical and thermoelectric behavior of orthorhombic $LaXO_3$ (X= Cr, Mn, Fe): For device application. Journal of Molecular Graphics and Modelling, 94 (2020) 107482.

[19] J. A. Mena, V. Mendoza-Estrada, EM Sabolsky, KA Sierros, and K Sabolsky, Exploring the impact of multivalent substitution on high-temperature electrical conductivity in doped lanthanum chromite perovskites: An experimental and ab-initio study. Journal of the European Ceramic Society, 44 (2024) 7040-7058

[20] Y. Zhou, Z. Lü, J. Li, S Xu, D Xu, and B Wei, The electronic properties and structural stability of $LaFeO_3$ oxide by niobium doping: A density functional theory study, International Journal of Hydrogen Energy, 46 (2021) 9193-9198.

[21] F. Hamioud, Saad Tariq, Abeeha Batool, and A. A. Mubarak, Theoretical investigation on orthorhombic $XMnO_3$ (X = Nd, Dy and Ho) perovskite manganates using DFT, Chemical Physics Letters, 760 (2020) 138005.

[22] S. Chandra, A. Biswas, M.-H. Phan, and H. Srikanth, Impacts of nanostructuring and magnetic ordering of Nd^{3+} on the magnetic and magnetocaloric response in $NdMnO_3$, J. Magn. Magn. Mater., 384 (2015) 138.

[23] Y. Wu, Q. Xie, M. Li, X. Sun, H.-L. Cai, and X.S. Wu, Structural and ferroelectric properties of orthogonal crystalline in Fe-doped $HoMnO_3$ synthesized at normal pressure, J. Mater. Sci. Mater. Electronics, 30 (2019) 7629.

[24] A. Munoz, J. A. Alonso, and M. J. Martinez-Lope, Magnetic structure evolution of $NdMnO_3$ derived from neutron diffraction data, J. García-Muñoz, M.T. Fernandez-Diaz J. Phys.: Condens. Matter, 12 (2000) 1361.

[25] M. Balli, S. Jandl, P. Fournier, and M. M. Gospodinov, Anisotropy-enhanced giant reversible rotating magnetocaloric effect in $HoMn_2O_5$ single crystals, Appl. Phys. Lett., 104 (2014) 232402

[26] Jin-Ling Jin, Xiang-Qun Zhang, Guo-Ke Li, Zhao-Hua Cheng, Lin Zheng, and Yi Lu, Giant anisotropy of magnetocaloric effect in $TbMnO_3$ single crystals, Phys. Rev. B, 83 (2011) 184431.

[27] M. Balli, S. Jandl, P. Fournier, S. Mansouri, A. Mukhin, Yu.V. Ivanov, and A.M. Balbashov, On the magnetocaloric effect in the multiferroic hexagonal $DyMnO_3$ single crystals, J. Magn. Magn. Mater,374 (2015) 252.

[28] Xiang-Qun Jin-Ling Jin, Heng Zhang, Ge, and Zhao-Hua Cheng, Rotating field entropy change in hexagonal $TmMnO_3$ single crystal with anisotropic paramagnetic response, Phys. Rev. B, 85 (2012) 214426.

[29] Takahiro Lingwei Li, Dexuan Namiki, Zhenghong Huo, Qian, and Katsuhiko Nishimura; Two successive magnetic transitions induced large refrigerant capacity in HoPdIn compound, Appl. Phys. Lett., 103 (2013) 222405.

[30] T. Kimura, T. Goto, H. Shintani, K. Ishizaka, T. Arima, and Y. Tokura, Magnetic control of ferroelectric polarization, Nature, 426 (2003) 55.

[31] A. Haoui, M. Elchikh, S. Hiadsi, and A. H. Baghdad, DFT analysis of mechanical, thermal, half-metallic, and thermoelectric properties of perovskites $PrMnO_3$ and $NdMnO_3$ ortho-manganite, Physica B: Condensed Matter 684 (2024) 416001.

[32] T. Z. Li, R. Khenata, and H. Khachai, DFT-Based Study on Electronic, Magnetic and Thermodynamic Properties of $HoMnO_3$: A Half-Metallic Material with Nearly Linear Band, Spin, 9 (2019) 1950017.

[33] M. Kumar, S. Shankar, A. Kumar, M. Jayasimhadri, and O. P. Thakur, Progress in multiferroic and magnetoelectric materials: applications, opportunities and challenges, J. Mater. Sci. Mater. Electron., 31 (2020) 19487.

[34] L. Jeuvrey, O. Peña, B. Moure, and C. Moure, Synthesis and magnetic properties of hexagonal $Y(Mn,Cu)O_3$ multiferroic materials, J. Magn. Magn. Mater., 324 (2012) 717.

[35] D. M. S. Brito, A. F. Lima, and M. V. Lalic, Photoferroic prospective of multiferroic $HoMnO_3$ compound, evaluated on the base of the DFT study of its magnetic, electronic, and optical properties, Journal of Physics and Chemistry of Solids, 177 (2023) 111301.

[36] Thomas Lottermoser, Thomas Lonkai, Uwe Amann, Dietmar Hohlwein, Jörg Ihringer and Manfred Fiebig, Magnetic phase control by an electric field Nature, 430 (2004) 541.

[37] B. Lorenz, F. Yen, M. Gospodinov and C. W. Chu, Field-induced phases in $HoMnO_3$ at low temperatures, Physical Review B, 71 (2005) 014438.

[38] B. Bouadjemi, S. Bentata, A. Abbad, and W. Benstaali, Ab-initio study of optoelectronic and magnetic properties of the orthorhombic $NdMnO_3$ perovskite, Solid State Communications, 207 (2015) 9-15.

[39] C. G. Zhong, Q. Jiang, J. H. Fang, and C. W. Ge, Magnetoelectric coupling and magnetoelectric properties of single-phase ABO_3 type multiferroic materials, Acta Phys. Sin., 58 (2009) 3491.

[40] A. M. Sousa, W. S. Coutinho, A. F. Lima, and M. V. Lalica, Structural, bonding, and electronic properties of the hexagonal ferroelectric and paraelectric phases of $LuMnO_3$ compound: A density functional theory study, J. Chem. Phys., 142 (2015) 074703.

[41] A. Sajawal, M. Ishfaq, G. Murtaza, I. Habib, N. Muhammad, and S. Sharif, Half metallic ferromagnetism in $PrMnO_3$ orthorhombic stable phase: an experimental and theoretical investigation. Materials Research Express, 5 (2018) 116103.

[42] Y. Zhou, Z. Lü, B. Wei, Z. Wang, and X. Zhu, Electronic structure and surface properties of $PrMnO_3$ (001): A density functional theory study. Solid State Communications, 201 (2015) 31-35.

[43] P. Blaha, K. Schwarz, G. K. H. Madsen, D. Kvasnicka, and J. Luitz, WIEN2K, an Augmented Plane Wave þ Local Orbitals Program for Calculating Crystal Properties, Karlheinz Schwarz, Techn. Universïtat Wien, Austria, 2001.

[44] W. Kohn, and L. J. Sham, Self-Consistent Equations Including Exchange and Correlation Effects, Phys. Rev. 140 (4A) (1965) 1133–1138.

[45] J.P. Perdew, S. Kurth, A. Zupan, and P. Blaha, Accurate Density Functional with Correct Formal Properties: A Step Beyond the Generalized Gradient Approximation, Phys. Rev. Lett. 82 (12) (1999) 2544–2547.

[46] V. I. Anisimov, J. Zaanen, and O. K. Andersen, Band theory and Mott insulators: Hubbard U instead of Stoner I, Phys. Rev. B, 44 (1991) 943

[47] G. K. Madsen, and D. J. Sing, BoltzTraP. A code for calculating band-structure dependent quantities, Comput. Phys. Commun., 175 (2006) 67.

[48] V. Tyuterev, and N. Vast, Murnaghan's equation of state for the electronic ground state energy, Comput. Mater. Sci. 38 (2006) 350.

[49] K. Momma, and I. Fujio, VESTA 3 for three-dimensional visualization of crystal, volumetric and morphology data, Journal of applied crystallography, 44.6 (2011) 1272-1276.

[50] Y. Selmani, H. Labrim, R. E. Bouayadi, and L. Bahmad, Effects of Mg doping on physical properties of zinc-blende mercury selenide HgSe compound. Physica B: Condensed Matter, 644 (2022) 414204.

[51] Y. Selmani, H. Labrim, and L. Bahmad, Effect of Mg substitution on structural, electronic, optical and thermoelectric properties of ZnTe alloy, Optik, 299 (2024) 171605.

[52] Y. A. Uspenskii, E. T. Kulatov, and S. V. Halilov, Effect of anisotropy on magneto-optical properties of uniaxial crystals: application to CrO_2, Phys. Rev. B 54 (1996) 474.

[53] S. Benyoussef, A. Jabar and L. Bahmad, « Biaxial and Uniaxial Tensile Strains Effects on Electronic, Optical, and Thermoelectric Properties of $ScBiTe_3$ Compound », Crystal Research and Technology, 58 (2023) 2300069.

[54] A. Jabar, S. Benyoussef and L. Bahmad, « On the Structural, Magnetic, Electronic, Optical, and Thermoelectric Characteristics of the Solar Perovskite $CsCdI_3$: DFT and SCAPS-1D Studies », Transactions on Electrical and Electronic Materials, (2024), doi: 10.1007/s42341-024-00532-5.